Comput. Methods Appl. Mech. Engrg. 198 (2008) 367–376

Contents lists available at ScienceDirect

Comput. Methods Appl. Mech. Engrg.

journal homepage: www.elsevier.com/locate/cma

A new method for the numerical solution of vorticity–streamfunction formulations

Sheng Chen, Jonas Tölke, Manfred Krafczyk *

Institute for Computational Modeling in Civil Engineering, Technical University, Braunschweig 38106, Germany

ARTICLE INFO

Article history:
Received 6 June 2008
Received in revised form 24 July 2008
Accepted 1 August 2008
Available online 28 August 2008

Keywords:
Lattice Boltzmann model
Vorticity–streamfunction

ABSTRACT

A lattice Boltzmann model for vorticity–streamfunction formulations is proposed in this paper. The present model was validated by several benchmark problems. Excellent agreement between the present results and other numerical data shows that this model is an efficient numerical method for the numerical solution of vorticity–streamfunction formulations.

1. Introduction

Computational fluid dynamic (CFD) methods have been developed for several decades, providing an efficient tool for the analysis of many fundamental and practical fluid dynamics problems. Various numerical techniques have been employed to solve the Navier–Stokes (N–S) equations that govern viscous fluid flow, by using the Euler description, in which the truncated domain of the entire flow region is overlaid by a grid system. Despite the standard CFD methods, which rely on solving equations of primitive-variables, the velocity and pressure, have achieved huge success on the simulation of complex fluid flow, vorticity formulations [1–4] are still widely used because the solution procedure is often advantageous when adapted to a specific formulation of a given problem (e.g. studies on geophysical flows and that on buoyancy-driven flows in crystal-growth melts) [5,6].

The use of vorticity formulations for the analysis of incompressible viscous fluid flows has several advantages. Some of these advantages include a reduction of the number of equations to be solved through the elimination of the pressure variable, identical satisfaction of the compressibility constraint and the continuity equation, and an implicitly higher order approximation of the velocity components [2–4,7]. The above reasons make vorticity formulations very attractive for the accurate solution of high Reynolds number planar or axisymmetric N–S equations, especially for studying vortex dominated flows where the vorticity field is known to play an important role in the dynamics of organized flow structures [8]. However, a few drawbacks still affect vorticity formulations. The most important seems the fact that the boundary conditions are typically given in terms of prescribed velocity rather than prescribed vorticity or vorticity flux. Several approaches have been developed over the years to derive vorticity boundary conditions from the prescribed velocity boundary conditions and the vorticity within the domain. Some of these approaches include vorticity–streamfunction methods [2,3], velocity–vorticity Cauchy methods [9], vorticity–velocity Poisson equation methods [10], Biot-Savart methods [11], and generalized Helmholtz decomposition methods [12]. Among them, the vorticity–streamfunction formulations are by far the ones most commonly used [1–3,13], ranging from hydrodynamics [2], geo- and astrophysics [14], biofluids [15] to optimal design of thermal systems [16,17]. Originally, the vorticity–streamfunction formulations were designed only for two-dimensional flows [18], but until now they have been extended to solve three-dimensional problems [8]. The advantages of vorticity–streamfunction formulations have been demonstrated previously using spectral methods [19], finite element methods [20], projection methods [21] and finite difference methods [22]. Recently, parallel computer implementations of vorticity formulations were developed to solve practical flows [7].

In the last two decades, the lattice Boltzmann model (LBM) has matured as an efficient alternative for simulating and modeling complicated physical, chemical and social systems [23–40]. The implementation of a LBM procedure is much easier than that of traditional numerical methods. Parallelization of the LBM is natural since the relaxation is local and the communication pattern in propagation is one way, and the performance increases nearly linearly with the number of CPUs. Moreover, the LBM has been compared favourably with spectral methods [41], artificial compressibility methods [42], finite volume methods [43,44] and finite difference methods [45], all quantitative results further validate excellent performance of the LBM not only in computational efficiency but also in computational accuracy. Due to these

* Corresponding author.
E-mail addresses: chen@irmb.tu-bs.de (S. Chen), toelke@irmb.tu-bs.de (J. Tölke), kraft@irmb.tu-bs.de (M. Krafczyk).

0045-7825/$ - see front matter © 2008 Published by Elsevier B.V.
doi:10.1016/j.cma.2008.08.007

advantages, the LBM has been successfully used to simulate many problems, from laminar single phase flows to turbulent multiphase flows [25,26].

However, all existing LBMs are designed for primitive-variable formulations of N–S equations. To the best knowledge of the authors, there is no attempt to extend the LBM to solve vorticity–streamfunction formulations. To employ the LB method in the fields where vorticity–streamfunction equations, instead of primitive-variables-based N–S equations, serving as the governing equations, it is necessary to design a LBM based on vorticity–streamfunction equations, which motivates the present study. Another obvious advantage of the vorticity–streamfunction-based LBM over primitive-variables-based LBMs is that potential forcing (e.g. gravity, electromagnetic forcing) can be eliminated from the problem in the same way that pressure is eliminated in the vorticity–streamfunction method [3,7]. It is well known that forcing treatment is a complicated process in classical primitive-variables-based LBMs [46,47]. Consequently for simulating flows with

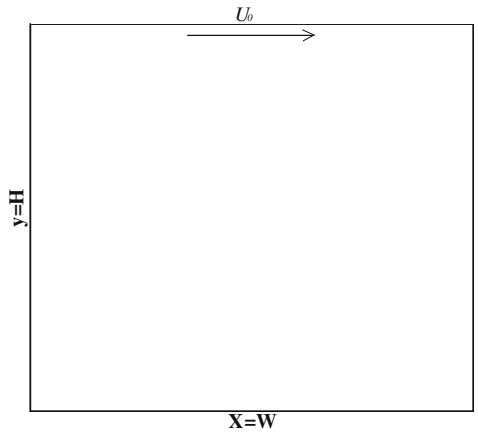

Fig. 1. Schematic of one-sided lid-driven flow in a rectangular cavity of aspect ratio J.

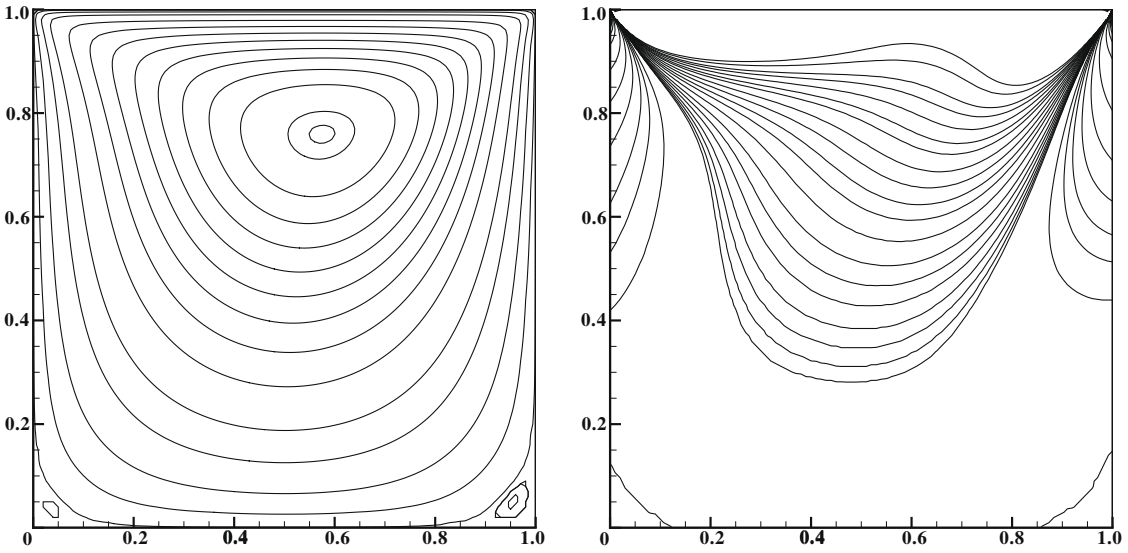

Fig. 2. Contour lines of ψ and ω of flow in one-sided lid-driven cavity: $Re = 50$, $J = 1$.

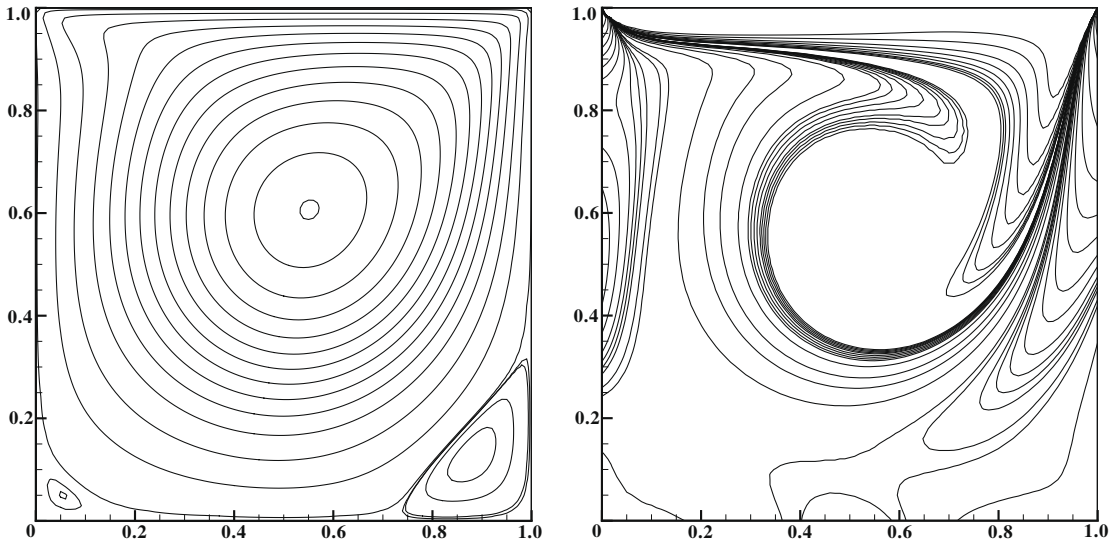

Fig. 3. Contour lines of ψ and ω of flow in one-sided lid-driven cavity: $Re = 400$, $J = 1$.

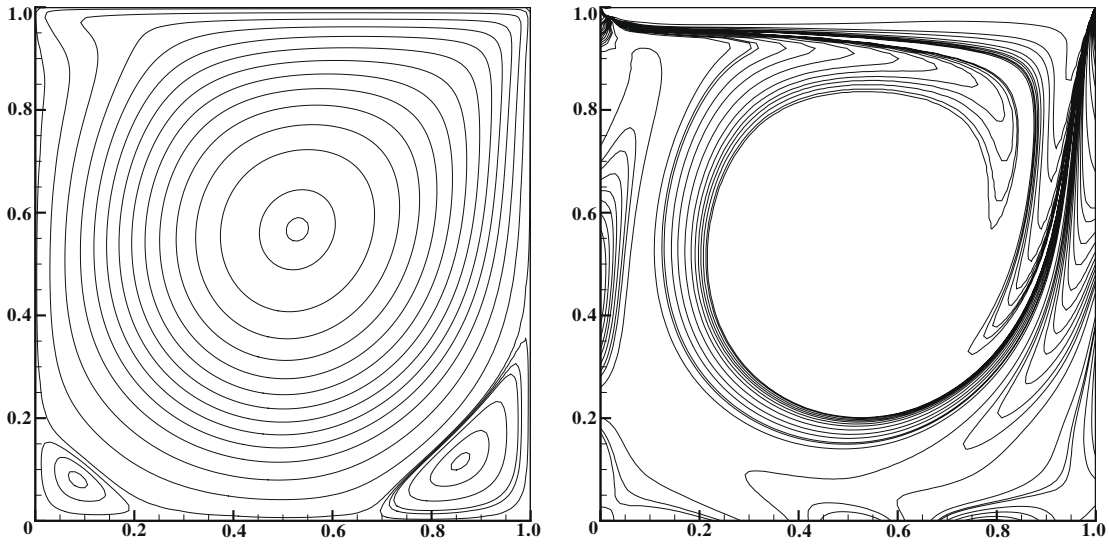

Fig. 4. Contour lines of ψ and ω of flow in one-sided lid-driven cavity: $Re = 1000$, $J = 1$.

potential forcing (e.g. Czochralski growth in an external magnetic field [6]), the present model is simpler and more efficient than primitive-variables-based LBMs [48,49] because such forcing vanishes in the vorticity–streamfunction-based governing equations.

The rest of this paper is organized as follows. Vorticity–streamfunction formulations for incompressible flows is presented in Section 2. In Section 3, a new LBM is introduced for the numerical solution of vorticity–streamfunction formulations. In Section 4, numerical experiments are performed to test the performance of the present model. The comparison of the computational efficiency between the present model and other methods is also made. Conclusion is presented in the last section.

2. Vorticity–streamfunction formulations for incompressible flows

For simplicity, in the present study we only focus on two-dimensional problems. Vorticity–streamfunction formulations for two-dimensional incompressible flows read [8]:

$$\frac{\partial \omega}{\partial t} + u\frac{\partial \omega}{\partial x} + v\frac{\partial \omega}{\partial y} = \frac{1}{Re}\left(\frac{\partial^2 \omega}{\partial x^2} + \frac{\partial^2 \omega}{\partial y^2}\right), \tag{1}$$

$$\frac{\partial^2 \psi}{\partial x^2} + \frac{\partial^2 \psi}{\partial y^2} = -\omega. \tag{2}$$

in the above equations Re is the Reynolds number. ψ and ω are the streamfunction and the vorticity, respectively. The velocities u and v are obtained from:

$$u = \frac{\partial \psi}{\partial y}, \tag{3}$$

$$v = -\frac{\partial \psi}{\partial x}. \tag{4}$$

3. Lattice Boltzmann model for vorticity–streamfunction formulations

Because Eq. (1) is nothing but a convection–diffusion equation, there are many matured efficient LBMs for this type of equation

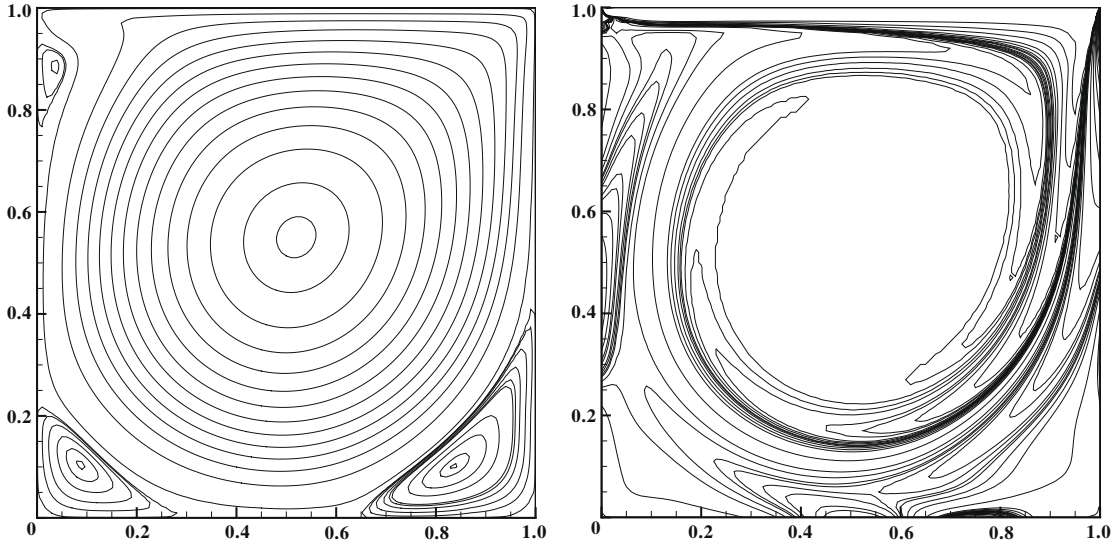

Fig. 5. Contour lines of ψ and ω of flow in one-sided lid-driven cavity: $Re = 2000$, $J = 1$.

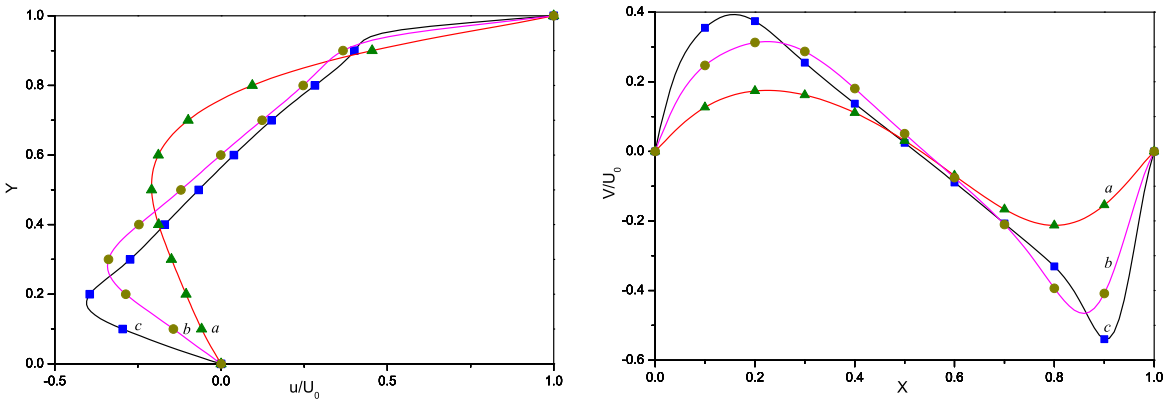

Fig. 6. The velocity components, u and v, along the vertical and horizontal lines through the square cavity center for the driven cavity flow at different Reynolds numbers. (a) $Re = 50$; (b) $Re = 400$ and (c) $Re = 1000$. Solid lines: present results; symbols: solution of Ref. [68].

[29,50–55]. In this paper, the D2Q5 model proposed in our previous work [51] for combustion simulation is employed. It reads:

$$g_k(\vec{x} + c\vec{e}_k\Delta t, t + \Delta t) - g_k(\vec{x}, t) = -\tau^{-1}[g_k(\vec{x}, t) - g_k^{(\mathrm{eq})}(\vec{x}, t)], \tag{5}$$

where $\vec{e}_k$ $(k = 0, \ldots, 4)$ are the discrete velocity directions:

$$\vec{e}_i = \begin{cases} (0,0): & i = 0, \\ (\cos(i-1)\pi/2, \sin(i-1)\pi/2): & i = 1,2,3,4. \end{cases}$$

$c = \Delta x/\Delta t$ is the fluid particle speed. Δx, Δt and τ are the lattice grid spacing, the time step and the dimensionless relaxation time, respectively.

The equilibrium distribution function $g_k^{(\mathrm{eq})}$ is defined by

$$g_k^{(\mathrm{eq})} = \frac{\omega}{5}\left[1 + 2.5\frac{\vec{e}_k \cdot \vec{u}}{c}\right]. \tag{6}$$

The vorticity is obtained by

$$\omega = \sum_{k\geqslant 0} g_k \tag{7}$$

Table 1
Locations of vortex of the one-sided lid-driven square cavity flow: $(\cdot)_c$ primary vortex; $(\cdot)_l$ lower left vortex; $(\cdot)_r$ lower right vortex

Re	x_c	y_c	x_l	y_l	x_r	y_r
50						
a	–	–	–	–	–	–
b	–	–	–	–	–	–
c	–	–	–	–	–	–
d	0.5781	0.7578	0.0468	0.0468	0.9609	0.0546
e	0.5796	0.7601	0.0440	0.0440	0.9551	0.0505
400						
a	0.5547	0.6055	0.0508	0.0469	0.8906	0.1250
b	0.5608	0.6078	0.0549	0.0510	0.8902	0.1255
c	0.5547	0.6094	0.0508	0.0469	0.8867	0.1250
d	0.5625	0.6133	0.0507	0.0507	0.8906	0.1289
e	0.5510	0.6100	0.0500	0.0500	0.8810	0.1298
1000						
a	0.5313	0.5625	0.0859	0.0781	0.8594	0.1094
b	0.5333	0.5647	0.0902	0.0784	0.8667	0.1137
c	0.5313	0.5625	0.0859	0.0781	0.8672	0.1172
d	0.5391	0.5703	0.0937	0.0859	0.8750	0.1250
e	0.5309	0.5699	0.0899	0.0800	0.8610	0.1180
2000						
a	–	–	–	–	–	–
b	0.5255	0.5490	0.0902	0.1059	0.8471	0.0980
c	0.5234	0.5469	0.0898	0.1016	0.8438	0.1016
d	–	–	–	–	–	–
e	0.5205	0.5501	0.0900	0.1010	0.8399	0.1009

Note: a, Ghia et al. [65]; b, Hou et al. [67]; c, Guo et al. [68]; d, Patil et al. [64]; e, present work.

and the dimensionless relaxation time τ is determined by the Reynolds number

$$Re = \frac{5}{2c^2(\tau - 0.5)}. \tag{8}$$

Eq. (2) is just the Poisson equation, which also can be effectively solved by the lattice Boltzmann method [56–61] or the multigrid method [62]. In the present study, the model proposed in Ref. [56] is employed because compared to others this model is more efficient and more accurate to solve the Poisson equation. The evolution equation for Eq. (2) reads [56]

$$f_k(\vec{x} + c\vec{e}_k\Delta t, t + \Delta t) - f_k(\vec{x}, t) = \Omega_k + \Omega_k', \tag{9}$$

where $\Omega_k = -\tau_\psi^{-1}[f_k(\vec{x}, t) - f_k^{(\mathrm{eq})}(\vec{x}, t)]$, $\Omega_k' = \Delta t\zeta_k\Theta D$ and $D = \frac{c^2}{2}(0.5 - \tau_\psi)$. τ_ψ is the dimensionless relaxation time, which can be chosen arbitrarily except 0.5 [56]. $f_k^{(\mathrm{eq})}$ is the equilibrium distribution function, and defined by

$$f_k^{(\mathrm{eq})} = \begin{cases} (\xi_0 - 1.0)\psi: & k = 0, \\ \xi_k\psi: & k = 1,2,3,4 \end{cases} \tag{10}$$

ξ_k and ζ_k are weight parameters given as $\xi_0 = 0$, $\xi_k = 1/4$ $(k = 1, \ldots, 4)$, $\zeta_0 = 0$, $\zeta_k = 1/4$ $(k = 1, \ldots, 4)$. ψ is obtained by

$$\psi = \frac{1}{1 - \xi_0}\sum_{k\geqslant 1} f_k. \tag{11}$$

The detailed derivation from Eqs. (5) and (9) to Eqs. (1) and (2) can be found in Refs. [51,56].

In the present model Eqs. (3) and (4) are solved by the central finite difference scheme. In our simulations, the convergence of Eq. (2) is very fast except during the early short period of simulations. Consequently the present model keeps high computational efficiency, as the results in Section 4 demonstrate.

Table 2
Comparison of the computational efficiency between different methods for the one-sided lid-driven square cavity flow

Re	Ref. [68]	Ref. [69]	Ref. [70]	Present
50				
Iterations	73900	2000	3700	2200
Time	921	743	468	291
400				
Iterations	89200	2000	4900	4500
Time	1082	1215	608	596
1000				
Iterations	93400	2000	6300	6100
Time	1139	1746	767	812

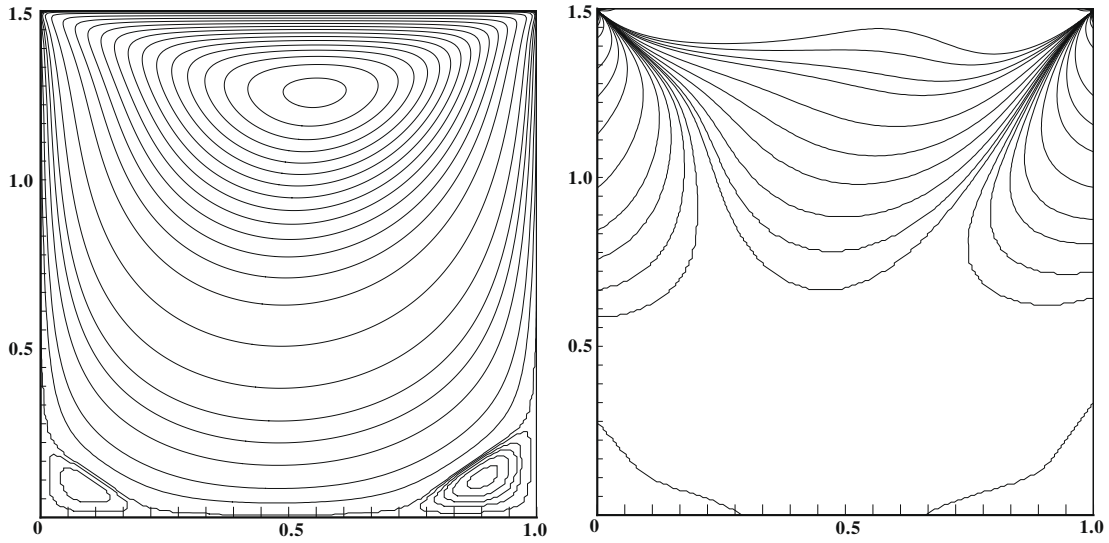

Fig. 7. Contour lines of ψ and ω of flow in one-sided lid-driven cavity: $Re = 50$, $J = 1.5$.

4. Numerical results and discussion

Flow in a rectangular one-sided lid-driven cavity is an interesting research problem because many important flow phenomena such as corner vortices, longitudinal vortices, Taylor–Görtler vortices, transition and turbulence all occur in the same closed geometry [22]. The configuration of flow is also relevant to a number of industrial applications [63,64]. Fig. 1 shows a schematic of a rectangular lid-driven cavity with aspect ratio $J = H/W$, H being the cavity-depth and W the width. There have been dozens of papers on this benchmark problem [22,65,66], besides that using LBMs [63,64,67,68], to cite only a few.

For one-sided lid-driven cavity flow, $u = v = 0$ on all walls except the top lid moving with velocity $u = U_0$. $\psi = 0$ and $\frac{\partial \psi}{\partial n} = 0$ on all walls, n means the normal direction of the wall. The values of ω on the stationary solid walls can be calculated by [8]

$$\omega = \frac{7\psi_w - 8\psi_{w-1} + \psi_{w-2}}{2\Delta n^2} \tag{12}$$

and those on the moving lid are calculated by [8]

$$\omega = \frac{7\psi_w - 8\psi_{w-1} + \psi_{w-2}}{2\Delta n^2} - \frac{3U_0}{\Delta n}, \tag{13}$$

where the subscript w means the nodes on the walls. The more detail description on boundary values of ψ and ω can be found in Ref. [8].

Firstly, the present model is validated by flow in a square cavity because there are fairly large number of studies conducted at $J = 1$. Figs. 2–5 illustrate the contour lines of ψ and ω of flows $50 \leqslant Re \leqslant 2000$, with the grid resolution 100×100. In order to get grid-independent numerical results, in this study we employed several different grid resolutions, from 80×80 to 256×256, and found that the grid resolution 100×100 is enough for such Reynolds number range. For higher Re, one must choose a finer grid resolution. For low $Re \leqslant 1000$, only three vortices appear in the cavity, a primary one near the center and a pair of secondary ones in the lower corners of the cavity. At $Re = 2000$, a third secondary vortex is seen in the upper left corner. We can also see that the center of the primary vortex moves toward the center of the cavity as Re increases. The velocity components, u and v, along the vertical

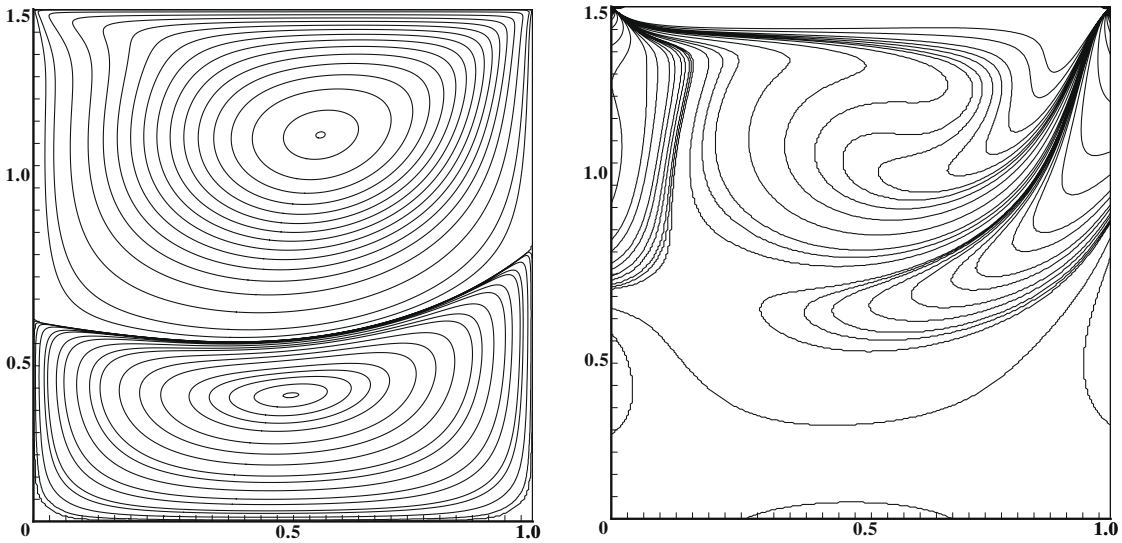

Fig. 8. Contour lines of ψ and ω of flow in one-sided lid-driven cavity: $Re = 400$, $J = 1.5$.

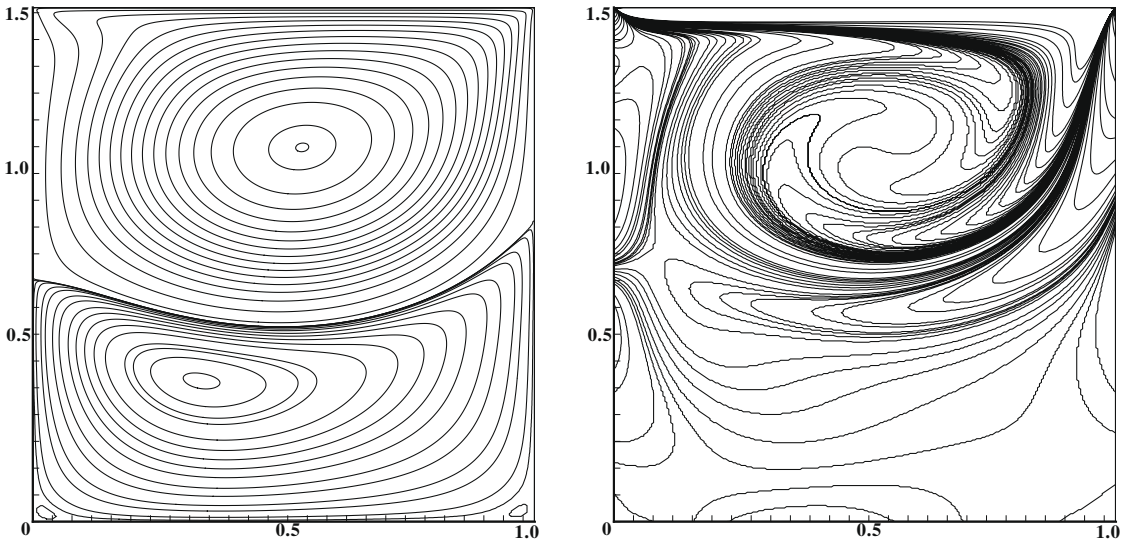

Fig. 9. Contour lines of ψ and ω of flow in one-sided lid-driven cavity: $Re = 1000$, $J = 1.5$.

Table 3
Locations of vortex of the one-sided lid-driven rectangle cavity flow, $J = 1.5$: $(\cdot)_{c1}$ first primary vortex; $(\cdot)_{c2}$ second primary vortex; $(\cdot)_l$ lower left vortex; $(\cdot)_r$ lower right vortex

Re	x_{c1}	y_{c1}	x_{c2}	y_{c2}	x_l	y_l	x_r	y_r
50								
a	0.5781	1.2578	–	–	0.0937	0.1015	0.8906	0.1406
b	0.5793	1.2581	–	–	0.0944	0.1000	0.8889	0.1391
400								
a	0.5625	1.1172	0.4453	0.3906	0.0312	0.0312	0.9843	0.0391
b	0.5708	1.1328	0.5004	0.3928	0.0310	0.0309	0.9827	0.0401
1000								
a	0.5352	1.0820	0.3007	0.4179	0.0352	0.0352	0.9648	0.0391
b	0.5363	1.0907	0.3059	0.4102	0.0395	0.0397	0.9648	0.0411

Note: a, Patil et al. [64]; b, present work.

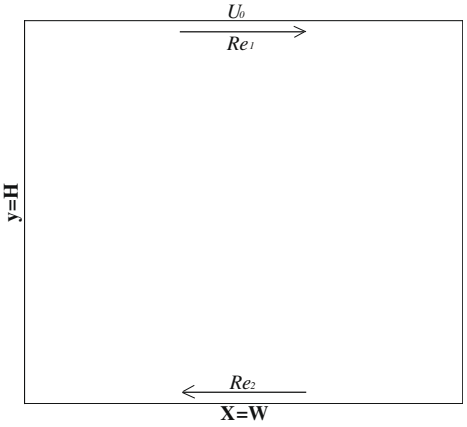

Fig. 11. Schematic of two-sided lid-driven flow in a rectangular cavity of aspect ratio *J*.

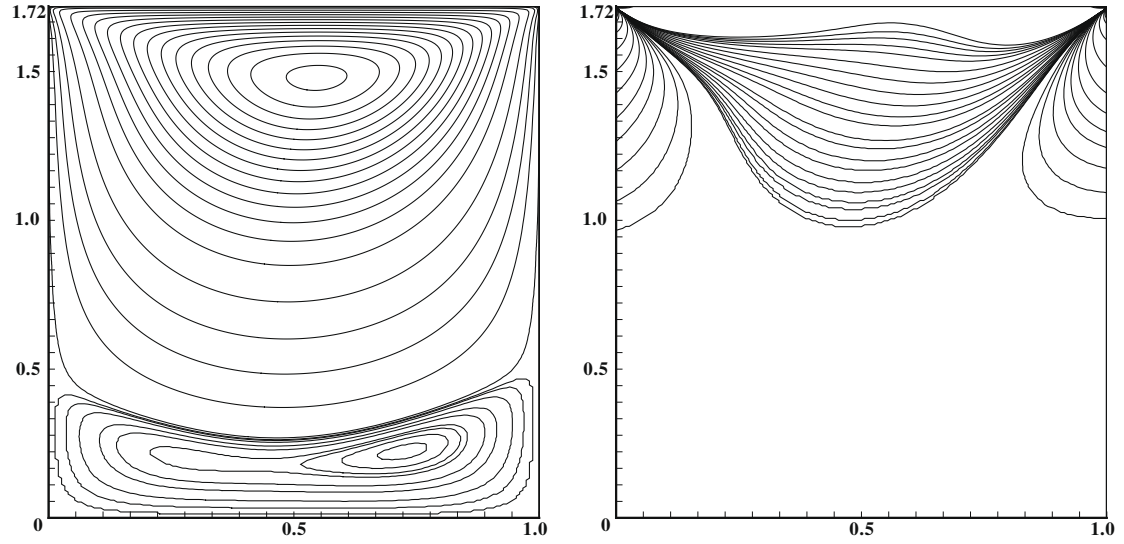

Fig. 10. Contour lines of ψ and ω of flow in one-sided lid-driven cavity: $Re = 50$, $J = 1.72$.

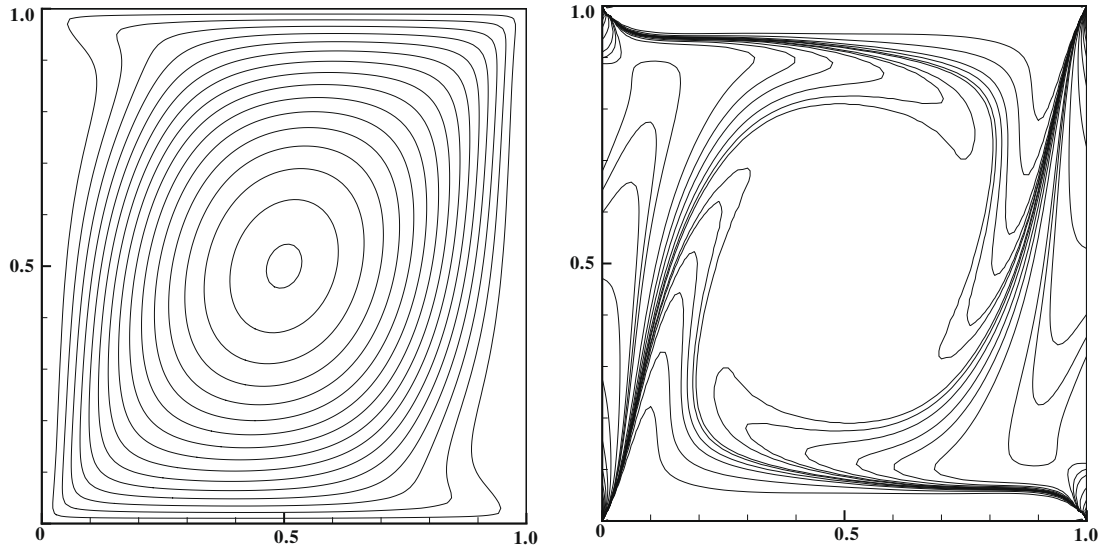

Fig. 12. Contour lines of ψ and ω of flow in two-sided lid-driven cavity $Re_1 = Re_2 = 400, J = 1.0$: antiparallel wall motion.

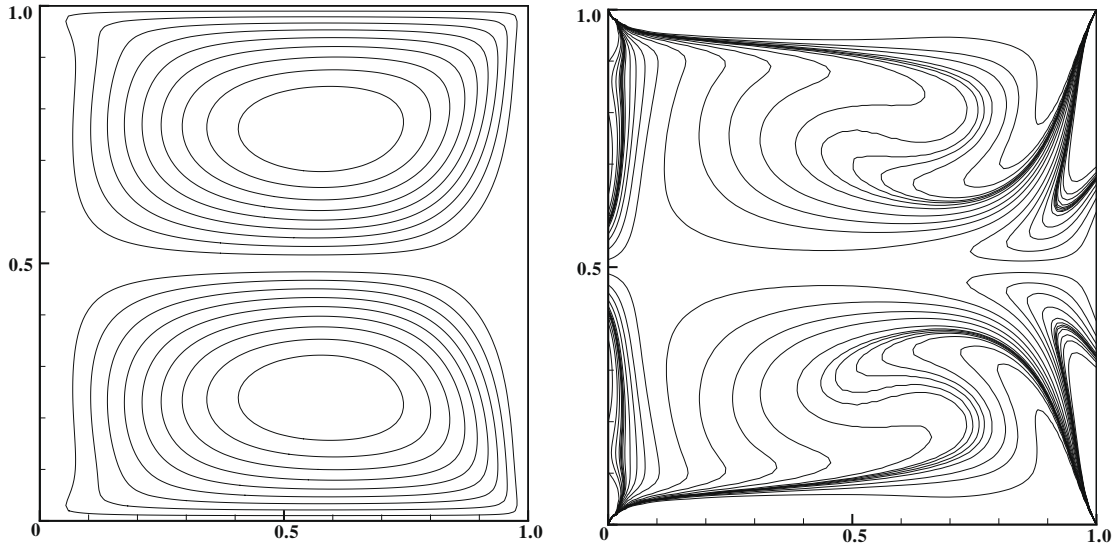

Fig. 13. Contour lines of ψ and ω of flow in two-sided lid-driven cavity $Re_1 = 400, Re_2 = -400, J = 1.0$: parallel wall motion.

and horizontal center lines for different *Re* are shown in Fig. 6. The profiles are found to become near linear in the center core of the cavity as *Re* becomes large. These observations show that the present simulation is in agreement with the previous studies [22,64,65,67,68].

To quantify the results, the locations of the primary center vortex and the two secondary ones are listed in Table 1. From the table, we can see that the locations of the vortices predicted by the present model agree well with those of previous work [64,65,67,68] for all the Reynolds numbers considered.

Table 2 shows the computational performance, number of iterative step and computational time (Unit second), of the present model, comparing with that of the latest computer source codes used in Refs. [68–70]. The computer source codes in Ref. [68,69] solving the primitive-variables-based N–S equations are based on the classical primitive-variables-based LB method and the projection method, respectively, while the computer source code in Ref.[70] solves the streamfunction–vorticity formulation by the finite difference method. The grid size 100×100, which is enough for lid-driven square cavity flows with $50 \leqslant Re \leqslant 1000$, was employed for all methods except the projection method which with the grid solution 48×48. For the methods in Refs. [68,70] and the present model, the computation process terminated when

$$\frac{\sum_{x,y}|\vec{u} - \vec{u}^*|}{\sum_{x,y}|\vec{u}^*|} < 10^{-5}, \tag{14}$$

where the superscript $*$ indicates the results obtained by Guo's LB model [68] with grid solution 256×256. For the projection method [69], the time step $\Delta t = 0.001$ and the final time is 2.0. All simulations were performed on a Pentium 4 (3.0G CPU). It is clear that in most cases the present model is the fastest, and always faster than the primitive-variables-based LBM.

In this study, we also simulated one-sided lid-driven flows in deep cavities ($J > 1$) which have been lately receiving increasing attention [63,64]. Figs. 7–9 show the contour lines of ψ and ω of flows $50 \leqslant Re \leqslant 1000$, $J = 1.5$. It can be seen from Figs. 7–9 that, a series of successive, counter-rotating vortices are formed below

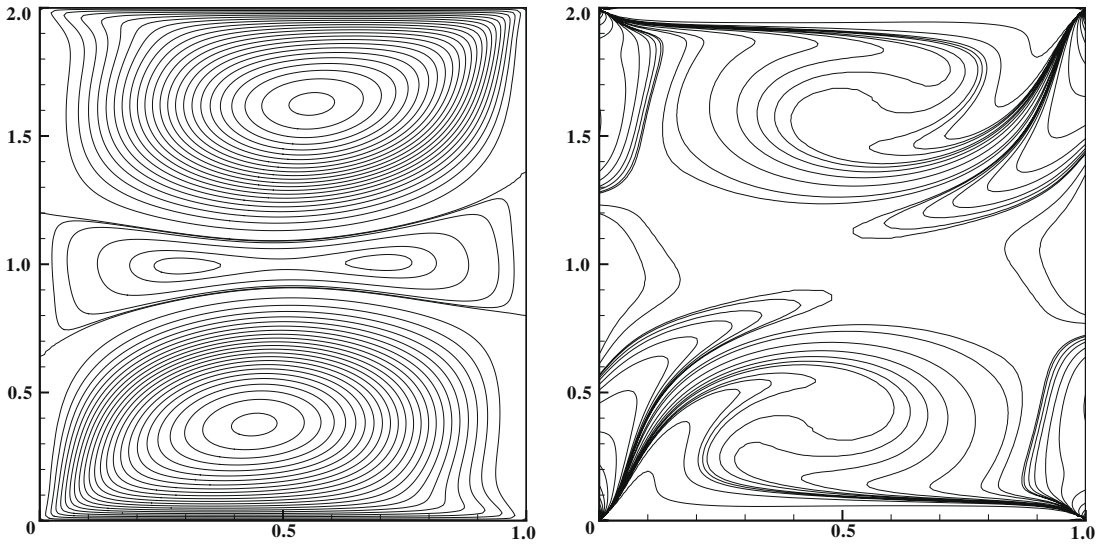

Fig. 14. Contour lines of ψ and ω of flow in two-sided lid-driven cavity $Re_1 = Re_2 = 700$, $J = 2.0$: antiparallel wall motion.

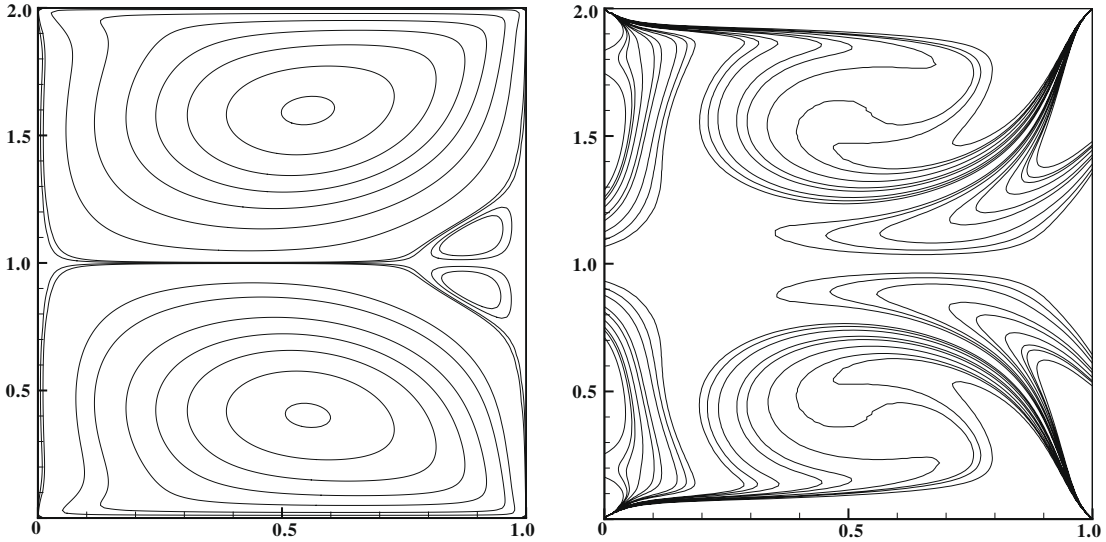

Fig. 15. Contour lines of ψ and ω of flow in two-sided lid-driven cavity $Re_1 = 700$, $Re_2 = -700$, $J = 2.0$: parallel wall motion.

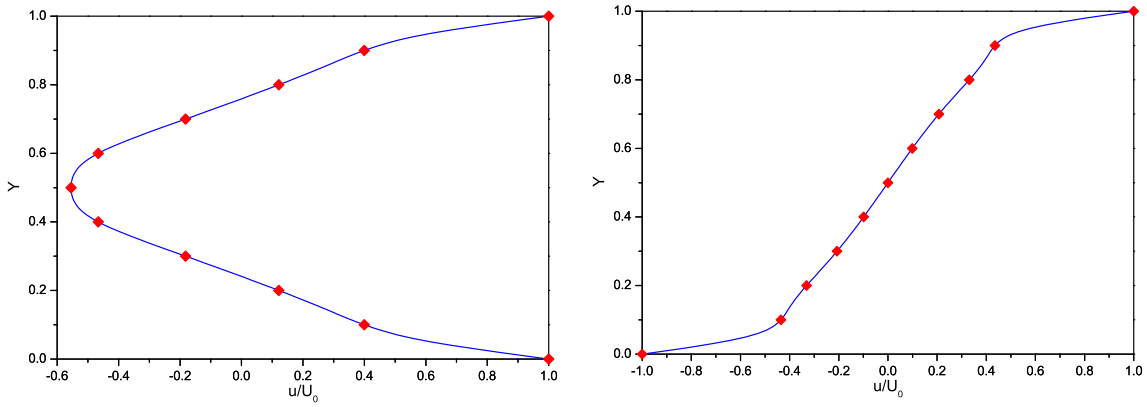

Fig. 16. The velocity component u, along the vertical line through the cavity center for the two-sided driven cavity flow $|Re_1| = |Re_2| = 400$, $J = 1.0$. (a) Parallel wall motion; (b) antiparallel wall motion. Solid lines: present results; symbols: solution obtained by Guo's model [68].

the moving lid. Further, as the Reynolds number increases, the center of the primary-eddy begins to move downwards, with respect to the top lid. This behavior is very similar to the flow in a square cavity. However, in the case of the deep cavity, the center of the primary vortex does not reach the geometric center of the cavity due to the evolution of a second primary-eddy at higher Reynolds numbers. Further, at low Reynolds numbers (e.g. Fig. 7) two stationary, corner eddies (also called "Moffatt eddies" [64]) are observed at the bottom of the cavity. When J attains a certain critical value, the two "Moffatt eddies" begin to coalesce together, as Fig. 10 shows (comparison with Fig. 7). These observations are in agreement with the previous publications [22,64].

Table 3 lists the locations of the first and the second primary vortices together with the two secondary ones, which also agree well with the previous data [64].

Finally, we simulated flow in a two-sided lid-driven cavity. In contrast to the fairly large number of studies conducted for one-sided lid-driven cavities, relatively little investigation has been carried out for flow in a two-sided lid-driven cavity which has been employed to study drying processes as well as polymer processing and thin film coating [71–74]. And the multiplicity of such flow is also a "hot" research field in fluid dynamics [71,74]. The top lid moves with velocity U_0 (Re_1) and the bottom lid moves in parallel ($-Re_2$) or in antiparallel (Re_2), as Fig. 11 illustrates.

Figs. 12–15 show the flow patterns of symmetrical driving, with different Reynolds number and aspect ratio. When both walls move in the same direction (parallel wall motion) with the same velocity ($Re_1 = -Re_2$) the induced vortices have opposite vorticity and the streamlines are symmetric with respect to the mid-plane of y coordinate. For antiparallel wall motion ($Re_1 = Re_2$) the near-wall vortices have the same sense of rotation and are well separated for sufficiently large aspect ratios, depending on Re. The vortices and the streamlines are point symmetric with respect to the geometric center of the cavity. All are in agreement with the previous publications [71,72,74]. Furthermore, the quantitative comparison of the values of velocity component u between that obtained by the present model and that got by other model [68] is illustrated in Fig. 16, which also agree very well each other.

5. Conclusion

In this study, we propose a LBM-based new method for the numerical solution of vorticity–streamfunction formulations. The excellent performance of the present model is demonstrated by several benchmark problems: flows in one-sided lid-driven square cavities, flows in one-sided lid-driven deep cavities and flows in two-sided lid-driven rectangular cavities. The fine structures of the flow patterns can be described by the present model. Especially, parallel computer implementations of the present model are easier than traditional numerical methods due to the intrinsic parallel advantage of the LBM. The comparison of the computational efficiency between the present model and other methods (including the classical primitive-variables-based LBM) shows that the computational efficiency of the present model is fairly higher than other methods. Moreover, it is well known that forcing treatment is a complicated process in classical primitive-variables-based LBMs. However, potential forcing can be eliminated from the problem in the same way that pressure is eliminated in the vorticity–streamfunction method. Theoretically the present model is much simpler and fairly more efficient than primitive-variables-based LBMs for simulating flows with potential forcing because such forcing vanishes in the vorticity–streamfunction-based governing equations, which will be validated by numerical simulations in the following study. Recently, we extended the present model for thermal flows and found that it works well for high Grashof number $Gr = 10^7$ with a relative low grid resolution 100×100, however the primitive-variables-based LBMs require finer grid resolution: grid resolution 150×150 for $Gr = 10^6$ and 474×474 for $Gr = 10^7$. The advantages of the present model appear more obviously in these cases.

Though the present model is designed for two-dimensional flows, its extension to three-dimensional problems, which seems conceptually straightforward but still appears entirely open, will be considered in future studies.

Acknowledgements

This work was partially supported by the Alexander von Humboldt Foundation, Germany. The authors gratefully acknowledge the referees for their helpful advice. The authors would also like to thank Prof. E. Erturk, Gebze Institute of Technology, Turkey and Prof. C. Pozrikidis, University of California, USA for sharing their computer source code. One of the authors (S. Chen) gratefully acknowledge Prof. B. Shi, Prof. Z. Guo and Dr. Z. Chai, Huazhong University of Science and Technology, China, for useful discussions and sharing their LB computer source code during this work.

References

[1] P. Chaviaropoulos, K. Giannakoglou, A vorticity–streamfunction formulation for steady incompressible two-dimensional flows, Int. J. Numer. Methods Fluids 23 (1996) 431–444.
[2] A.J. Majda, A. Bertozzi, Vorticity and Incompressible Flow, Cambridge University Press, Cambridge, 2001.
[3] S. Orszag, M. Israeli, Numerical simulation of viscous incompressible flows, Ann. Rev. Fluid Mech. 6 (1974) 281–318.
[4] L. Quartapelle, Numerical Solution of the Incompressible Navier–Stokes Equations, Birkhäuser, Basle, 1983.
[5] G.J.F. van Heijst, H.J.H. Clercx, Laboratory modeling of geophysical vortices, Ann. Rev. Fluid Mech. 41 (2009) 143–164.
[6] W.E. Langlois, Buoyancy-driven flows in crystal-growth melts, Ann. Rev. Fluid Mech. 17 (1985) 191–215.
[7] M.J. Brown, M.S. Ingber, Parallelization of a vorticity formulation for the analysis of incompressible viscous fluid flows, Int. J. Numer. Methods Fluids 39 (2002) 979–999.
[8] T.J. Chung, Computational Fluid Dynamics, Cambridge University Press, Cambridge, 2002.
[9] T.B. Gatski, C.E. Grosch, M.E. Rose, The numerical solution of the Navier–Stokes equations for 3-dimensional, unsteady, incompressible flows by compact schemes, J. Comput. Phys. 82 (1989) 298–329.
[10] O. Daube, Resolution of the 2D Navier–Stokes equations in velocity–vorticity form by means of an influence matrix technique, J. Comput. Phys. 103 (1992) 402–414.
[11] A.J. Chorin, J.E. Marsden, A Mathematical Introduction to Fluid Mechanics, Springer Verlag, Berlin, 1990.
[12] L. Morino, Helmholtz decomposition revisited: vorticity generation and trailing edge condition, Comput. Mech. 1 (1986) 65–90.
[13] T.E. Tezduyar, J. Liou, D.K. Ganjoo, M. Behr, Solution techniques for the vorticity–streamfunction formulation of two-dimensional unsteady incompressible flows, Int. J. Numer. Methods Fluids 11 (1990) 515–539.
[14] H. Schamel, N. Das, Scalar vortex dynamics of incompressible fluids and plasmas in Lagrangian space, Phys. Plasmas 8 (2001) 3120–3123.
[15] G. Pontrelli, Blood flow through an axisymmetric stenosis, Proc. Inst. Mech. Engrg. Part H, J. Engrg. Med. 215 (2001) 1–10.
[16] A.C. Baytas, Entropy generation for natural convection in an inclined porous cavity, Int. J. Heat Mass Transfer 43 (2000) 2089–2099.
[17] W.J. Luo, R.J. Yang, Multiple fluid flow and heat transfer solutions in a two-sided lid-driven cavity, Int. J. Heat Mass Transfer 50 (2007) 2394–2405.
[18] A. Thom, The flow past a circular cylinders at low speeds, Proc. Roy. Soc., Lond. Sect. A 141 (1933) 651–669.
[19] R. Peyret, Spectral Methods for Incompressible Viscous Flow, Springer Verlag, New York, 2002.
[20] E. Barragy, G.F. Carey, Stream function–vorticity driven cavity solution using p finite elements, Comput. Fluids 26 (1997) 455–468.
[21] O. Botella, R. Peyret, Benchmark spectral results on the lid-driven cavity flow, Comput. Fluids 27 (1998) 421–433.
[22] P.N. Shankar, M.D. Deshpande, Fluid mechanics in the driven cavity, Ann. Rev. Fluid Mech. 32 (2000) 93–136.
[23] Y. Qian, D. d'Humieres, P. Lallemand, Lattice BGK models for Navier–Stokes equation, Europhys. Lett. 17 (1992) 479–484.
[24] R. Benzi, S. Succi, M. Vergassola, The lattice Boltzmann equation: theory and applications, Phys. Report. 222 (1992) 145–197.
[25] S. Chen, G.D. Doolen, Lattice Boltzmann method for fluid flows, Ann. Rev. Fluid Mech. 30 (1998) 29–364.

[26] S. Succi, The Lattice Boltzmann Equation for Fluid Dynamics and Beyond, Oxford University Press, Oxford, 2001.
[27] R.J. Goldstein, W.E. Ibele, S.V. Patankar, et al., Heat transfer – A review of 2003 literature, Int. J. Heat Mass Transfer 49 (2006) 451–534.
[28] S. Succi, E. Foti, F. Higuera, Three-dimensional flows in complex geometries with the lattice Boltzmann method, Europhys. Lett. 10 (1989) 433–438.
[29] S. Chen, S.P. Dawson, G.D. Doolen, et al., Lattice methods and their applications to reacting systems, Comput. Chem. Engrg. 19 (1995) 617–646.
[30] H. Chen, S. Kandasamy, S. Orszag, et al., Science 301 (2003) 633–636.
[31] Y. Qian, S. Succi, S. Orszag, Recent advances in lattice Boltzmann computing, Ann. Rev. Comput. Phys. 3 (1995) 195–242.
[32] G. Hazi, A.R. Imre, G. Mayer, et al., Lattice Boltzmann methods for two-phase flow modeling, Ann. Nucl. Energy 29 (2002) 1421–1453.
[33] D. Yu, R. Mei, L.S. Luo, et al., Viscous flow computations with the method of lattice Boltzmann equation, Prog. Aerospace Sci. 39 (2003) 329–367.
[34] M.C. Sukop, D.T. Thorne Jr., Lattice Boltzmann Modeling: An Introduction for Geoscientists and Engineers, Springer, Heidelberg, Berlin, New York, 2006.
[35] S. Chakraborty, D. Chatterjee, An enthalpy-based hybrid lattice-Boltzmann method for modelling solid–liquid phase transition in the presence of convective transport, J. Fluid Mech. 592 (2007) 155–175.
[36] S. Chen, Z. Liu, Z. He, et al., A new numerical approach for fire simulation, Int. J. Mod. Phys. C 18 (2007) 187–202.
[37] Z. Guo, C. Zheng, B. Shi, Lattice Boltzmann equation with multiple effective relaxation times for gaseous microscale flow, Phys. Rev. E 77 (2008) 036707-1–036707-12.
[38] D. Raabe, Overview of the lattice Boltzmann method for nano- and microscale fluid dynamics in materials science and engineering, Model. Simul. Mater. Sci. Engrg. 12 (2004) 13–46.
[39] J. Meng, Y. Qian, X. Li, et al., Lattice Boltzmann model for traffic flow, Phys. Rev. E 77 (2008) 036108-1–036108-9.
[40] K. Furtado, J.M. Yeomans, Lattice Boltzmann simulations of phase separation in chemically reactive binary fluids, Phys. Rev. E 73 (2006) 066124-1–066124-7.
[41] D.O. Martinez, W.H. Matthaeus, S. Chen, et al., Comparison of spectral method and lattice Boltzmann simulations of two-dimensional hydrodynamics, Phys. Fluids 6 (1994) 1285–1298.
[42] X. He, G.D. Doolen, T. Clark, Comparison of the lattice Boltzmann method and the artificial compressibility method for Navier–Stokes equations, J. Comput. Phys. 179 (2002) 439–451.
[43] Y.Y. Al-Jahmany, G. Brenner, P.O. Brunn, Comparative study of lattice-Boltzmann and finite volume methods for the simulation of laminar flow through a 4:1 planar contraction, Int. J. Numer. Methods Fluids 46 (2004) 903–920.
[44] A. Al-Zoubi, G. Brenner, Comparative study of thermal flows with different finite volume and lattice Boltzmann schemes, Int. J. Mod. Phys. C 15 (2004) 307–319.
[45] T. Seta, E. Takegoshi, K. Okui, Lattice Boltzmann simulation of natural convection in porous media, Math. Comput. Simulat. 72 (2006) 195200.
[46] Z. Guo, C. Zheng, B. Shi, Discrete lattice effects on the forcing term in the lattice Boltzmann method, Phys. Rev. E 65 (2002) 046308-1–046308-6.
[47] J.M. Buick, C.A. Greated, Gravity in a lattice Boltzmann model, Phys. Rev. E 61 (2000) 5307–5320.
[48] H. Huang, T.S. Lee, C. Shu, Hybrid lattice Boltzmann finite-difference simulation of axisymmetric swirling and rotating flows, Int. J. Numer. Methods Fluids 53 (2007) 1707–1726.
[49] Y. Peng, C. Shu, Y.T. Chew, J. Qiu, Numerical investigation of flows in Czochralski crystal growth by an axisymmetric lattice Boltzmann method, J Comput. Phys. 186 (2003) 295–307.
[50] X. Zhang, A.G. Bengough, J.W. Crawford, I.M. Young, A lattice BGK model for advection and anisotropic dispersion equation, Adv. Water Res. 25 (2002) 1–8.
[51] S. Chen, Z. Liu, C. Zhang, et al., A novel coupled lattice Boltzmann model for low Mach number combustion simulation, Appl. Math. Comput. 193 (2007) 266–284.
[52] H.J. Liu, C. Zou, B.C. Shi, et al., Int. J. Heat Mass Transfer 49 (2006) 4672–4680.
[53] Z.L. Guo, B.C. Shi, C.G. Zheng, A lattice BGK model for the Bouessinesq equation, Int. J. Numer. Fluids 39 (2002) 325–342.
[54] I. Ginzburg, Equilibrium-type and link-type lattice Boltzmann models for generic advection and anisotropic-dispersion equation, Adv. Water Res. 28 (2005) 1171–1195.
[55] I. Ginzburg, Generic boundary conditions for lattice Boltzmann models and their application to advection and anisotropic dispersion equations, Adv. Water Res. 28 (2005) 1196–1216.
[56] Z. Chai, B. Shi, A novel lattice Boltzmann model for the Poisson equation, Appl. Math. Modell. (2007), doi:10.1016/j.apm.2007.06.033.
[57] X. He, N. Ling, Lattice Boltzmann simulation of electrochemical systems, Comput. Phys. Commun. 129 (2000) 158–166.
[58] Z. Guo, T.S. Zhao, Y. Shi, A lattice Boltzmann algorithm for electro-osmotic flows in microfluidic devices, J. Chem. Phys. 122 (2005) 144907.
[59] Z. Chai, Z. Guo, B. Shi, Study of electro-osmotic flows in microchannels packed with variable porosity media via lattice Boltzmann method, J. Appl. Phys. 101 (2007) 104913-1–104913-8.
[60] J. Wang, M. Wang, Z. Li, Lattice Poisson-Boltzmann simulations of electro-osmotic flows in microchannels, J. Colloid. Interface Sci. 296 (2006) 729–736.
[61] M. Hirabayashi, Y. Chen, H. Ohashi, The lattice BGK model for the Poisson equation, JSME Int. J. Ser. B 44 (1) (2001) 45–52.
[62] S. Melchionna, S. Succi, Electrorheology in nanopores via lattice Boltzmann simulation, J. Chem. Phys. 120 (2004) 4492–4497.
[63] M. Cheng, K.C. Hung, Vortex structure of steady flow in a rectangular cavity, Comput. Fluids 35 (2006) 1046–1062.
[64] D.V. Patil, K.N. Lakshmisha, B. Rogg, Lattice Boltzmann simulation of lid-driven flow in deep cavities, Comput. Fluids 35 (2006) 1116–1125.
[65] U. Ghia, K. Ghia, C. Shin, High-Re solutions for incompressible flow using Navier–Stokes equations and a multigrid method, J. Comput. Phys. 48 (1982) 387–411.
[66] F. Pan, A. Acrivos, Steady flows in rectangular cavities, J. Fluid Mech. 28 (1967) 643–655.
[67] S. Hou, Q. Zou, S. Chen, G. Doolen, A.C. Cogley, Simulation of cavity flow by the lattice Boltzmann method, J. Comput. Phys. 118 (1995) 329–347.
[68] Z.L. Guo, B.C. Shi, N.C. Wang, Lattice BGK model for incompressible Navier–Stokes equation, J. Comput. Phys. 165 (2000) 288–306.
[69] C. Pozrikidis, Fluid Dynamics: Theory, Computation, and Numerical Simulation, Accompanied by the Software Library FDLIB. Kluwer (Springer), Heidelberg, Berlin, New York, 2001. Computer source code could be donwloaded from <http://dehesa.freeshell.org/FDLIB/fdlib.shtml>.
[70] E. Erturk, T.C. Corke, C. Gokcol, Numerical solutions of 2-D steady incompressible driven cavity flow at high reynolds numbers, Int. J. Numer. Methods Fluids 48 (2005) 747–774. Computer source code could be donwloaded from <http://www.cavityflow.com>.
[71] S. Albensoeder, H.C. Kuhlmann, H.J. Rath, Multiplicity of steady two-dimensional flows in two-sided lid-driven cavities, Theoret. Comput. Fluid Dyn. 14 (2001) 223–241.
[72] E.M. Wahba, Multiplicity of states for two-sided and four-sided lid driven cavity flows, Comput. Fluids (2008), doi:10.1016/j.compfluid.2008.02.001.
[73] R.K. Tiwari, M.K. Das, Heat transfer augmentation in a two-sided lid-driven differentially heated square cavity utilizing nanofluids, Int. J. Heat Mass Transfer 50 (2007) 2002–2018.
[74] CH. Blohm, H.C. Kuhlmann, The two-sided lid-driven cavity: experiments on stationary and time-dependent flows, J. Fluid Mech. 450 (2002) 67–95.